

## Quantum phase transitions driven by rhombic-type single-ion anisotropy in the $S = 1$ Haldane chain

Yu-Chin Tzeng (曾郁欽),<sup>1,2,\*</sup> Hiroaki Onishi (大西弘明),<sup>3,†</sup> Tsuyoshi Okubo (大久保毅),<sup>4</sup> and Ying-Jer Kao (高英哲)<sup>2,5,‡</sup>

<sup>1</sup>Department of Physics, National Chung-Hsing University, Taichung 40227, Taiwan

<sup>2</sup>Department of Physics, National Taiwan University, Taipei 10617, Taiwan

<sup>3</sup>Advanced Science Research Center, Japan Atomic Energy Agency, Tokai, Ibaraki 319-1195, Japan

<sup>4</sup>Department of Physics, University of Tokyo, Tokyo 113-0033, Japan

<sup>5</sup>National Center for Theoretical Sciences, National Tsing Hua University, Hsinchu 300, Taiwan

(Received 17 May 2017; revised manuscript received 2 July 2017; published 3 August 2017)

The spin-1 Haldane chain is an example of the symmetry-protected-topological (SPT) phase in one dimension. Experimental realization of the spin chain materials usually involves both the uniaxial-type,  $D(S^z)^2$ , and the rhombic-type,  $E[(S^x)^2 - (S^y)^2]$ , single-ion anisotropies. Here, we provide a precise ground-state phase diagram for a spin-1 Haldane chain with these single-ion anisotropies. Using quantum numbers, we find that the  $\mathbb{Z}_2$  symmetry breaking phase can be characterized by double degeneracy in the entanglement spectrum. Topological quantum phase transitions take place on particular paths in the phase diagram, from the Haldane phase to the large- $E_x$ , large- $E_y$ , or large- $D$  phases. The topological critical points are determined by the level spectroscopy method with a newly developed parity technique in the density matrix renormalization group [Phys. Rev. B **86**, 024403 (2012)], and the Haldane-large- $D$  critical point is obtained with an unprecedented precision,  $(D/J)_c = 0.9684713(1)$ . Close to this critical point, a small rhombic single-ion anisotropy  $|E|/J \ll 1$  can destroy the Haldane phase and bring the system into a  $y$ -Néel phase. We propose that the compound  $[\text{Ni}(\text{HF}_2)(3\text{-Clpy})_4]\text{BF}_4$  is a candidate system to search for the  $y$ -Néel phase.

DOI: 10.1103/PhysRevB.96.060404

**Introduction.** Quantum magnetism of integer-spin chains has been attracting attention for decades. It was stimulated by the Haldane conjecture [1] that the lowest excitation in the antiferromagnetic Heisenberg model is gapped if and only if the spin  $S$  is an integer. Experimental evidences for the Haldane gap were discovered in several  $S = 1$  quasi-one-dimensional (Q1D) materials, e.g.,  $\text{CsNiCl}_3$  [2,3],  $\text{Y}_2\text{BaNiO}_5$  [4–6],  $\text{Ni}(\text{C}_2\text{H}_8\text{N}_2)_2\text{NO}_2(\text{ClO}_4)$  (NENP) [7,8], and  $[\text{Ni}(\text{C}_2\text{H}_8\text{N}_2)_2\text{NO}_2]\text{BF}_4$  (NENB) [9]. Due to the crystal field and the spin-orbit coupling, the microscopic effective Hamiltonian for the Q1D spin chains involves the single-ion anisotropies,

$$H = J \sum_{i=1}^L \vec{S}_i \cdot \vec{S}_{i+1} + D \sum_{i=1}^L (S_i^z)^2 + E \sum_{i=1}^L [(S_i^x)^2 - (S_i^y)^2], \quad (1)$$

where  $J > 0$  is the strength of the Heisenberg exchange interaction, as well as  $D$  and  $E$  are the parameters of the uniaxial and rhombic single-ion anisotropies, respectively. The Haldane gap is robust against small anisotropies, and it extends to a region so-called Haldane phase. In the absence of a local order, the Haldane phase falls beyond the paradigm of Landau's theory of phase transitions. From a topological point of view, the Haldane phase is classified as the symmetry-protected-topological (SPT) phase [10] for odd  $S$ , while the Haldane phase is adiabatically connected with a topological trivial phase for even  $S$  [11–15]. Interesting properties such as the valence-bond-solid (VBS) description

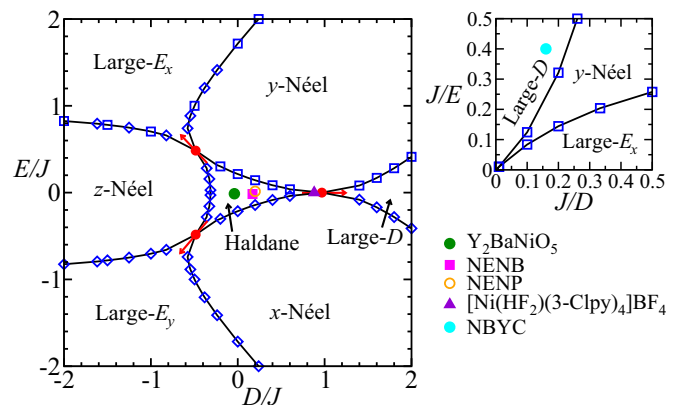


FIG. 1. Quantum phase diagram for the  $S = 1$  Haldane chain with both uniaxial and rhombic single-ion anisotropies. Topological quantum phase transitions occur through particular (red arrows) routes. The Haldane-large- $D$  critical point  $(D/J)_c = 0.9684713(1)$  is determined by the LS+DMRG method. A small rhombic anisotropy  $|E|/J \ll 1$  at this point  $(D/J)_c$  induces a transverse antiferromagnetic order.

[16], hidden  $\mathbb{Z}_2 \times \mathbb{Z}_2$  symmetry breaking, nonlocal string order, fractionalized gapless edge modes, and the degenerate entanglement spectra are used to characterize the SPT phase. On the other hand, the entanglement spectrum is not required to be degenerate for both the topological trivial phase and the symmetry breaking phase.

Prior theoretical and numerical investigations focus on the effects of the uniaxial anisotropy ( $D$  term) [17–26]. The effect of rhombic anisotropy ( $E$  term) lacks a complete theoretical understanding [27,28]; however, materials with large  $D/J$  and  $E/J$  are discovered, e.g., the  $S = 1$  Q1D chains,  $\text{Sr}_3\text{NiPtO}_6$  [29,30],  $\text{Ni}(\text{C}_2\text{H}_8\text{N}_2)_2\text{Ni}(\text{CN})_4$

\*d102054002@mail.nchu.edu.tw

†onishi.hiroaki@jaea.go.jp

‡yjkao@phys.ntu.edu.tw

TABLE I. The values of zero-field-splitting parameters for some spin-1 Q1D materials.

| Compounds  | $D/J$  | $E/J$     | Phase      | Ref.    |
|--|--------|-----------|------------|---------|
| $\text{Y}_2\text{BaNiO}_5$                             | -0.039 | -0.0127   | Haldane    | [4]     |
| NENB   | 0.17   | -0.016    | Haldane    | [9]     |
| NENP   | 0.2    | 0.01-0.02 | Haldane    | [8]     |
| $[\text{Ni}(\text{HF}_2)(3\text{-Clpy})_4]\text{BF}_4$ | 0.88   |           |            | [32,33] |
| NBYC <sup>a</sup>                                      | 6.25   | 2.5       | Large- $D$ | [34]    |
| NBYC <sup>b</sup>                                      | 7.49   | 4.26      | Large- $D$ | [35]    |
| NENC   | 7.5    | 0.83      | Large- $D$ | [31]    |
| $\text{Sr}_3\text{NiPtO}_6$                            | 8.8    | 0         | Large- $D$ | [29,30] |

<sup>a</sup>Susceptibility.

<sup>b</sup>An additional bilinear-biquadratic term is considered.

(NENC) [31],  $[\text{Ni}(\text{HF}_2)(3\text{-Clpy})_4]\text{BF}_4$  (py=pyridine) [32,33], and  $\text{Ni}(\text{C}_{10}\text{H}_8\text{N}_2)_2\text{Ni}(\text{CN})_4 \cdot \text{H}_2\text{O}$  (NBYC) [34-36].

In this Rapid Communication, we fill up the vacancy in the survey of the phase diagram regarding the  $E$  term. By means of the DMRG [37], within the periodic boundary conditions (PBC), the ground-state phase diagram of the  $S = 1$  Hamiltonian Eq. (1) is shown in Fig. 1, and some of spin-1 Q1D materials are listed in Table I. By the permutations of spin operators, the phase diagram shows a “rotational” symmetry in the rescaled  $D\text{-}\sqrt{3}E$  parameter space [38]. The Hamiltonian does not conserve the magnetization  $M = \sum_i S_i^z$  because of the  $E$  term. Instead of the magnetization, the parity of  $M$  is conserved.  $m = M \bmod 2 = 0$  or 1 is a good quantum number since the  $E$  term raises or lowers the magnetization by 2. The spatial inversion  $p = \pm 1$  and time reversal  $t = \pm 1$  are also good quantum numbers. We label the energy eigenstates and the entanglement states by these quantum numbers  $(m, p, t)$ . The number of states kept  $K$  is up to 2000 in this study.

**Energy and Entanglement Spectrum.** The Haldane phase surrounded by the other phases is a SPT phase [10] protected by the dihedral group, the time reversal, and the space-inversion symmetries [11,22]. The ground state can be described by the VBS picture [16]: Each spin-1 in the chain is regarded as triplet states of two spin-1/2, and the neighboring spin-1/2 of different spin-1 form a valence bond, the singlet state. From the VBS picture, two consequences are inferred. First, because each singlet contributes odd quantum numbers for both spatial inversion and time reversal, a closed chain of even number of singlets has quantum numbers  $(m, p, t) = (0, 1, 1)$ . Therefore, we compute the ground state energy  $E_g = E_0(0, 1, 1; \text{PBC})$  in this sector. Second, with the Haldane gap in the bulk, an open chain has free unpaired spin-1/2 states at the edges. For the PBC, a closed chain in our case, the edge states can be artificially created by the partial trace of one part of the bipartition. Explicitly, the chain is divided into two subsystems A and B with equal sizes, and the reduced density matrix  $\rho_A = \text{Tr}_B |\psi_0\rangle\langle\psi_0|$  is computed in the DMRG, where  $|\psi_0\rangle$  is the ground state. The entanglement spectrum is defined by  $\xi_i = -\ln \omega_i$ , where  $\omega_i$  is the  $i$ th largest eigenvalue of  $\rho_A$ . The edge states reflect on that the reduced state can be decomposed into the product  $\rho_A \approx (\frac{1}{2}\mathbb{1}_{2 \times 2}) \otimes \rho_0 \otimes (\frac{1}{2}\mathbb{1}_{2 \times 2})$  [39,40], where  $\mathbb{1}_{2 \times 2}$  are the two-by-two identity matrices of the edges, the boundary between A and B, and  $\rho_0$  is a pure-state bulk-part matrix of the subsystem A. This fact ensures a fourfold degenerate

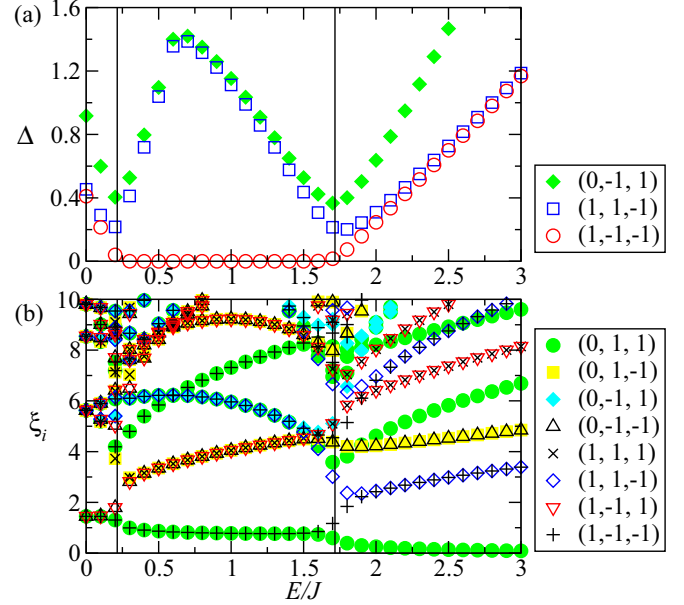


FIG. 2. (a) The excitation gap  $\Delta = E_0(m, p, t; \text{PBC}) - E_g$ , where  $E_g = E_0(0, 1, 1; \text{PBC})$  is the ground state energy. The ground state in the  $y$ -Néel phase has double degeneracy. (b) The entanglement spectra of at least fourfold, double, and nondegeneracy characterize the Haldane, the  $y$ -Néel, and the large- $E_x$  phases, respectively. The vertical lines indicate two critical points  $(E/J)_c \simeq 0.214$  and  $1.717$ , respectively. DMRG data for  $D/J = 0$  and  $L = 80$  are presented.  $K = 1000$  states are kept.

entanglement spectrum in the Haldane phase. The fourfold degeneracy can be seen as a simple illustration of the bulk-edge correspondence in the entanglement spectrum [41-43].

The lowest energy excitations and the low-lying entanglement spectra are shown in Fig. 2 for fixed  $D/J = 0$ . The Haldane gap is estimated as  $0.41J$  for  $D = E = 0$ , which agrees with recent numerical results [44]. Double degeneracy in the ground-state energy and the entanglement spectrum are found in the region between the Haldane phase and the large- $E_x$  phase. Both of the double degeneracies come from the nature of a  $\mathbb{Z}_2$  spontaneous symmetry breaking phase, with breaking the parity of magnetization, space inversion, and time-reversal symmetries, simultaneously. The spin-spin correlation shows the phase also breaks translational symmetry, as we will see in Fig. 3, therefore we refer to this phase as the  $y$ -Néel phase.

The degeneracy structure of entanglement spectrum has been proposed to distinguish different many-body quantum phases recently [22,43,45-47]. The reason of the double degeneracy in the  $y$ -Néel phase, Fig. 2(b), is that the degenerate ground state is selected as an eigenstate of the symmetry operators by the quantum numbers  $(m, p, t)$  in the DMRG [14]. Such an enforced symmetrized state is similar to a Greenberger-Horne-Zeilinger (GHZ) state, and the artificial double degenerate spectrum is generated. For example, the state  $\frac{1}{\sqrt{2}}(|\nearrow\nearrow\nearrow\rangle \pm |\searrow\searrow\searrow\rangle)$  has the inversion parity quantum number  $p = \pm 1$ , and it is an entangled state. However, each symmetry breaking state,  $|\nearrow\nearrow\nearrow\rangle$  or  $|\searrow\searrow\searrow\rangle$ , is not an eigenstate of the symmetry operator, and it is not entangled,

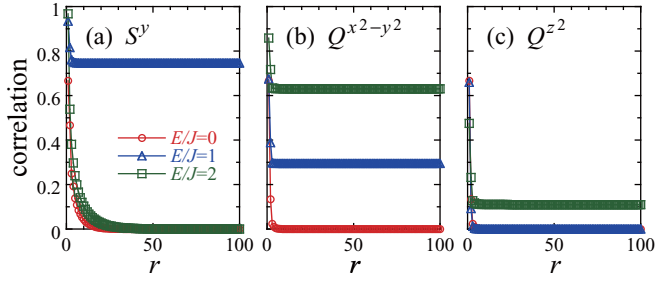


FIG. 3. Spin and quadrupole correlation functions at typical values of  $E/J$  for  $D/J = 0$  and  $L = 200$ . (a)  $(-1)^r \langle S_0^y S_r^y \rangle$ , (b)  $\langle Q_0^{x^2-y^2} Q_r^{x^2-y^2} \rangle$ , and (c)  $\langle Q_0^{z^2} Q_r^{z^2} \rangle$ . Note that  $r = 100$  for the most distant sites in the periodic chain of  $L = 200$ .

either. Note that the double degeneracy appears in the entire spectrum and is also found in the  $z$ -Néel and  $x$ -Néel phases. Thus, the degeneracy structure of the entanglement spectrum identifies the SPT phase (fourfold), the  $\mathbb{Z}_2$  symmetry breaking phase (double), and the topological trivial phase (single).

In the  $z$ -Néel phase, the parity of magnetization  $m$  is conserved, therefore the other parity quantum numbers  $(p, t)$  are essential for observing the degenerate spectrum. In contrast, in the  $y$ -Néel (or  $x$ -Néel) phase, the double degeneracy can be observed when only using the parity of magnetization. Therefore the  $E$  term serves an ideal model Hamiltonian to observe the parity degeneracy in the spontaneous symmetry breaking phase. From the technical point of view, quantum numbers are usually used in the DMRG for preventing the mixture of different subspaces as well as stabilizing and accelerating the computations. Because the magnetization is the most often used quantum number in the DMRG, programming with the parity of magnetization should be easier than the parity of inversion or time reversal.

**Correlation Functions.** The microscopic spin states of novel quantum phases induced by single-ion anisotropies can be clarified by measuring spin correlation functions,  $\langle S_0^\alpha S_r^\alpha \rangle$ , and quadrupole correlation functions,  $\langle Q_0^\gamma Q_r^\gamma \rangle$ , where  $Q_i^{x^2-y^2} = (S_i^x)^2 - (S_i^y)^2$  and  $Q_i^{z^2} = \frac{1}{\sqrt{3}}[3(S_i^z)^2 - 2]$  are relevant quadrupole operators. In Fig. 3, we show typical behavior with increasing  $E/J$  for fixed  $D/J = 0$ . In the Haldane phase for small anisotropies, spin and quadrupole correlations are short ranged, as shown for  $E/J = 0$ . At intermediate  $E/J$ , robust antiferromagnetic correlations of the spin  $y$  component occur, as shown for  $E/J = 1$ . Spin correlations of the  $x$  and  $z$  components are short ranged (not shown). Note here that the local spin state is forced to be the lowest-energy eigenstate of  $E[(S_i^x)^2 - (S_i^y)^2]$ , given by  $|S_i^x = 0\rangle$ , where the local spin fluctuates in the  $yz$  plane. Such fluctuating spins align antiferromagnetically, while they preferably point to the  $y$  direction due to the  $E$  term. Thus the  $y$ -Néel phase is identified.

At large  $E/J$ , the ground state turns to be the product of  $|S_i^x = 0\rangle$ , and the Néel structure vanishes, as shown for  $E/J = 2$ . This phase is referred to as the large- $E_x$  phase. Because the negative  $E/J$  is equivalent to exchanging the  $x$  axis and  $y$  axis,  $E[(S_i^y)^2 - (S_i^x)^2]$ , we refer to the phase as the large- $E_y$  phase for the product of  $|S_i^y = 0\rangle$  at large negative  $E/J$ , and only positive  $E/J$  is discussed. A distinct feature for

the large- $E_x$  phase is that  $|S_i^x = 0\rangle$  has quadrupole moments,  $\langle Q_i^{x^2-y^2} \rangle = -1$  and  $\langle Q_i^{z^2} \rangle = \frac{1}{\sqrt{3}}$ , so that finite quadrupole correlations come out. The  $Q^{x^2-y^2}$  correlation develops in the  $y$ -Néel and large- $E_x$  phases, while the  $Q^{z^2}$  correlation grows after entering the large- $E_x$  phase. We should note that the  $E$  and  $D$  terms have the same forms as  $Q^{x^2-y^2}$  and  $Q^{z^2}$ , respectively, indicating emergent quadrupole degrees of freedom. We expect that the competition of quadrupole states would drive the system into quadrupole phases, the so-called spin nematic phases, but Néel phases are observed in the present case at zero magnetic field. The search for possible quadrupole phases in magnetic field would be an interesting future problem, since those in a spin-1/2 frustrated chain in high magnetic field have been actively discussed [48–53].

**Level Spectroscopy.** The critical points are determined by the finite size scaling of the entanglement entropy [38,54–57] and the level spectroscopy (LS) method. All the transitions belong to the Ising universality class with the central charge  $c = \frac{1}{2}$ , except three Gaussian points with  $c = 1$  labeled by the red points in Fig. 1. Topological quantum phase transitions occur at these Gaussian points, from the Haldane phase to the large- $D$ , large- $E_x$ , or large- $E_y$  phases. The topological quantum phase transition from the Haldane phase to the large- $D$  phase is known as an example of the third-order Gaussian transition [21], therefore this critical point is more difficult to be precisely determined than the conventional second-order transitions. Several methods for the determination of this critical point were investigated, including the LS plus exact diagonalization (LS+ED) [17], fidelity susceptibility [20,21], quantum Monte Carlo (QMC) [58], von Neumann entropy [59], and the quantum renormalization group [60]. Here we use the parity DMRG [14] to perform the LS+DMRG method.

The LS method [61–66] is based on the effective field theory of the sine-Gordon model and the  $c = 1$  conformal field theory. The critical point can be probed by the energy level crossing within the twisted boundary conditions (TBC),  $S_{L+1}^x \rightarrow -S_1^x$ ,  $S_{L+1}^y \rightarrow -S_1^y$ ,  $S_{L+1}^z \rightarrow S_1^z$ . The LS method can be roughly described by the VBS picture [66], as shown in Fig. 4. For the TBC chain with even length  $L$ , there are odd number of singlet bonds and one triplet bond in the Haldane phase. Each singlet contributes the inversion parity quantum number  $p_i = -1$ , and the triplet bond contributes  $p_L = 1$ . Thus, the quantum number for the system becomes odd,  $p = \prod_{i=1}^L p_i = -1$ . On the other hand, the inversion parity quantum number for the large- $D$  phase is always even,  $p = 1$ . Therefore, the Haldane phase and the large- $D$  phase are characterized

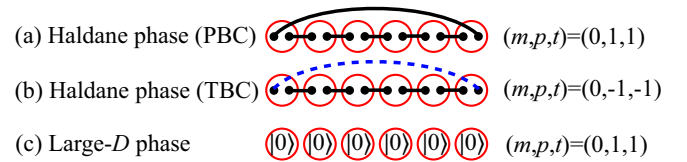


FIG. 4. (a) For a closed chain with even number of singlets, the quantum numbers for the Haldane phase are  $(m, p, t) = (0, 1, 1)$ . (b) Within TBC, the number of singlets become odd, and the quantum numbers change as  $(m, p, t) = (0, -1, -1)$ . (c) For large single-ion anisotropy, the quantum numbers are  $(m, p, t) = (0, 1, 1)$ .

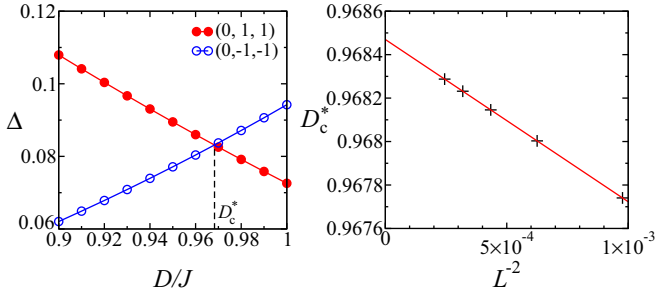


FIG. 5. (Left) Energy level crossing with different quantum numbers occurs at  $D_c^*$  for  $L = 64$ ,  $E/J = 0$ , within TBC.  $\Delta = E_0(m, p, t; \text{TBC}) - E_g$  and  $E_g = E_0(0, 1, 1; \text{PBC})$  is the ground state energy within PBC. (Right) Extrapolation of the critical point is performed by linear fitting.  $(D/J)_c = 0.9684713(1)$  is obtained.  $K = 2000$  states are kept.

by the energy  $E_0(0, -1, -1; \text{TBC})$  and  $E_0(0, 1, 1; \text{TBC})$ , respectively.

We show the energy level crossing  $E_0(m, p, t; \text{TBC})$  with different quantum numbers  $(m, p, t) = (0, 1, 1)$  and  $(0, -1, -1)$  in Fig. 5. The location of the crossing point is labeled by  $D/J = D_c^*$ , and the critical point is obtained by the extrapolation to the thermodynamic limits. It is known that the scaling formula is a polynomial function in  $L^{-2}$  [61–66]. This importantly makes the convergence fast, because the sub-leading term  $L^{-4}$  is much smaller than the leading term. Our numerical data [38], for  $L = 32, 40, 48, 56$ , and  $64$ , show that a linear fitting is good enough for the extrapolation. We obtain  $(D/J)_c = 0.96847133(2)$  with linear fitting and  $(D/J)_c = 0.96847141(2)$  with the subleading term  $L^{-4}$ . Therefore it would be safe to conclude  $(D/J)_c = 0.9684713(1)$  with the systematic error about  $10^{-7}$ . Although our LS+DMRG only have sizes  $L \leq 64$ , combining the DMRG technique proposed by Hu *et al.* [59] for large systems with level spectroscopy should further improve the precision of the value  $(D/J)_c$ . Other combinations such as LS+QMC [67] are also possible.

Finally, we briefly discuss the effect of  $E$  term at these (red points in Fig. 1) topological critical points. Basically, the effect of  $E$  term can be understood from the scaling dimension of the  $E$  term at the Haldane-large- $D$  critical point  $(D/J)_c$  in the renormalization group flow analysis. If the  $E$  term is relevant at the critical point, the critical point disappears by introducing an infinitesimal  $E$  term as observed in the phase diagram in the  $D$ - $E$  plane, Fig. 1. The Haldane-large- $D$  critical point  $(D/J)_c$  is characterized by the central charge  $c = 1$  free boson conformal field theory [18]. Note that the  $E$  term can be transformed as

$$E \sum_{i=1}^L [(S_i^x)^2 - (S_i^y)^2] = \frac{E}{2} \sum_{i=1}^L [(S_i^+)^2 + (S_i^-)^2]. \quad (2)$$

Thus, if the scaling dimension of  $(S_i^+)^2$  at the critical fixed point is less than the dimension  $1 + 1 = 2$ , the  $E$  term is relevant and an infinitesimal  $E/J$  flows away from the critical point. The renormalization flow may eventually goes to  $x$ - or  $y$ -Néel phases depending on the sign of  $E/J$ . Actually, a recent DMRG calculation has estimated the scaling dimension  $\Delta_s$  corresponding to this operator as  $\Delta_s = 0.750 \pm 0.002$  [18].

Because the scaling dimension clearly satisfies the relation  $\Delta_s < 2$ , we can conclude that the effect of  $E$  term is relevant at the Haldane-large- $D$  critical fixed point  $(D/J)_c$ . Thus we expect that by introducing infinitesimal  $E/J$ , the critical point between the Haldane and the large- $D$  phases disappears because the relevant  $E$  term increases along renormalization and it flows away from the critical point. By considering the symmetries of permutation of axis [38], the present discussions are also applicable for the critical points between the Haldane phase and large- $E_x$  or large- $E_y$  phases.

*Discussions.* We have investigated and provided a precise quantum phase diagram for the  $S = 1$  Haldane chain with both uniaxial and rhombic single-ion anisotropies, Eq. (1). By the parity DMRG [14] within PBC, we show that the symmetry breaking phase has double degeneracy in the entire entanglement spectrum. This generalizes the perspective that the degeneracy structure of entanglement spectrum tells different quantum phases, from the SPT phases to the symmetry breaking phases. The Haldane-large- $D$  critical point is determined by the LS+DMRG method with an unprecedented accurate value  $(D/J)_c = 0.9684713(1)$ . The presented power of the LS+DMRG method supports the reliability of finding the SPT intermediate- $D$  phase in the  $S = 2$   $XXZ$  chain [12–14]. From the phase diagram, we point out that a small rhombic anisotropy induces a transverse antiferromagnetic long range order when  $D/J$  is close to this  $(D/J)_c$ . This suggests that  $[\text{Ni}(\text{HF}_2)(3\text{-Clpy})_4]\text{BF}_4$ , with  $D/J \simeq 0.88$  [32], is either a possible candidate system to search for the  $y$ -Néel phase, or a candidate for observing the quantum phase transition driven by the rhombic-type single-ion anisotropy.

In the end of this Rapid Communication, we argue the spin-1 chain can be made by arranging the single-molecule magnets (SMM), e.g., CoH, the  $S = 1$  SMM [68]. We mention that recent experiments on a small cluster of SMMs have been taking into account the weak interactions between SMMs for  $L = 2$  [69] and  $L = 4$  [70]. On the other hand, atomic engineering has been able to tune the magnetic anisotropy [71] and tune the spin state by absorbing hydrogen [68,72]. The spin-spin interaction coming from the superexchange mechanism [73–76] and the Ruderman-Kittel-Kasuya-Yosida (RKKY) interaction [77] have been observed. Cold rubidium atoms have recently been proposed to simulate a spin-1 chain with uniaxial-type single-ion anisotropy [78]. In principle, an artificial spin chain with both uniaxial and rhombic single-ion anisotropies can be created.

*Acknowledgments.* Y.C.T. and Y.J.K. are grateful to MOST in Taiwan via No. MOST105-2112-M-002-023-MY3. H.O. acknowledges the support of JSPS KAKENHI Grant No. JP16K05494. We are grateful to the National Center for High-performance Computing for computer time and facilities. Computations were also done on the supercomputers at the Japan Atomic Energy Agency and the Institute for Solid State Physics, the University of Tokyo. We are grateful to H. Zhai, K.-K. Ng, M. Ternes, and M. Meisel for many useful discussions. T.O. was supported by JSPS KAKENHI Grant No. JP15K17701 and by MEXT of Japan as a social and scientific priority issue (creation of new functional devices and high-performance materials to support next-generation industries; CDMSI) to be tackled by using a post-K computer.

- [1] F. D. M. Haldane, Nonlinear Field Theory of Large-Spin Heisenberg Antiferromagnets: Semiclassically Quantized Solitons of the One-Dimensional Easy-Axis Néel State, *Phys. Rev. Lett.* **50**, 1153 (1983).
- [2] W. J. L. Buyers, R. M. Morra, R. L. Armstrong, M. J. Hogan, P. Gerlach, and K. Hirakawa, Experimental Evidence for the Haldane Gap in a Spin-1 Nearly Isotropic, Antiferromagnetic Chain, *Phys. Rev. Lett.* **56**, 371 (1986).
- [3] M. Kenzelmann, R. A. Cowley, W. J. L. Buyers, Z. Tun, R. Coldea, and M. Enderle, Properties of Haldane excitations and multiparticle states in the antiferromagnetic spin-1 chain compound CsNiCl<sub>3</sub>, *Phys. Rev. B* **66**, 024407 (2002).
- [4] G. Xu, J. F. DiTusa, T. Ito, K. Oka, H. Takagi, C. Broholm, and G. Aeppli, Y<sub>2</sub>BaNiO<sub>5</sub>: A nearly ideal realization of the  $S = 1$  Heisenberg chain with antiferromagnetic interactions, *Phys. Rev. B* **54**, R6827 (1996).
- [5] C. Rudowicz, P. Gnutek, S. Kimura, M. Açıkgöz, and Y. Y. Yeung, Modeling spectroscopic properties of Ni<sup>2+</sup> ions in the Haldane gap system Y<sub>2</sub>BaNiO<sub>5</sub>, *Appl. Magn. Reson.* **44**, 899 (2013).
- [6] P. Gnutek, M. Açıkgöz, and C. Rudowicz, Tools for magnetostructural correlations for the  $3d^8$  (<sup>3</sup>A<sub>2</sub> state) ions at orthorhombic sites: Comparative study with applications to Ni<sup>2+</sup> ions in Y<sub>2</sub>BaNiO<sub>5</sub> and Nd<sub>2</sub>BaNiO<sub>5</sub>, *J. Magn. Magn. Mater.* **374**, 484 (2015).
- [7] J. P. Renard, M. Verdager, L. P. Regnault, W. A. C. Erkelens, J. Rossat-Mignod, and W. G. Stirling, Presumption for a quantum energy gap in the quasi-one-dimensional  $S = 1$  Heisenberg antiferromagnet Ni(C<sub>2</sub>H<sub>8</sub>N<sub>2</sub>)<sub>2</sub>NO<sub>2</sub>(ClO<sub>4</sub>), *Europhys. Lett.* **3**, 945 (1987).
- [8] L. P. Regnault and J. P. Renard, Spin dynamics in the Haldane-gap system NENP, *Physica B* **215**, 71 (1995).
- [9] E. Čížmár, M. Ozerov, O. Ignatchik, T. P. Papageorgiou, J. Wosnitza, S. A. Zvyagin, J. Krzystek, Z. Zhou, C. P. Landee, B. R. Landry, M. M. Turnbull, and J. L. Wikaira, Magnetic properties of the Haldane-gap material [Ni(C<sub>2</sub>H<sub>8</sub>N<sub>2</sub>)<sub>2</sub>NO<sub>2</sub>](BF<sub>4</sub>), *New J. Phys.* **10**, 033008 (2008).
- [10] Z.-C. Gu and X.-G. Wen, Tensor-entanglement-filtering renormalization approach and symmetry-protected topological order, *Phys. Rev. B* **80**, 155131 (2009).
- [11] F. Pollmann, E. Berg, A. M. Turner, and M. Oshikawa, Symmetry protection of topological phases in one-dimensional quantum spin systems, *Phys. Rev. B* **85**, 075125 (2012).
- [12] T. Tonegawa, K. Okamoto, H. Nakano, T. Sakai, K. Nomura, and M. Kaburagi, Haldane, large- $D$ , and intermediate- $D$  states in an  $S = 2$  quantum spin chain with on-site and XXZ anisotropies, *J. Phys. Soc. Jpn.* **80**, 043001 (2011).
- [13] K. Okamoto, T. Tonegawa, and T. Sakai, Ground-state phase diagram of the bond-alternating  $S = 2$  quantum spin chain with the XXZ and on-site anisotropies – symmetry protected topological phase versus trivial phase –, *J. Phys. Soc. Jpn.* **85**, 063704 (2016).
- [14] Y.-C. Tzeng, Parity quantum numbers in the density matrix renormalization group, *Phys. Rev. B* **86**, 024403 (2012).
- [15] J. A. Kjäll, M. P. Zaletel, R. S. K. Mong, J. H. Bardarson, and F. Pollmann, Phase diagram of the anisotropic spin-2 XXZ model: Infinite-system density matrix renormalization group study, *Phys. Rev. B* **87**, 235106 (2013).
- [16] I. Affleck, T. Kennedy, E. H. Lieb, and H. Tasaki, Rigorous Results on Valence-Bond Ground States in Antiferromagnets, *Phys. Rev. Lett.* **59**, 799 (1987).
- [17] W. Chen, K. Hida, and B. C. Sanctuary, Ground-state phase diagram of  $S = 1$  XXZ chains with uniaxial single-ion-type anisotropy, *Phys. Rev. B* **67**, 104401 (2003).
- [18] C. D. E. Boschi, E. Ercolessi, F. Ortolani, and M. Roncaglia, On  $c=1$  critical phases in anisotropic spin-1 chains, *Eur. Phys. J. B* **35**, 465 (2003).
- [19] L. C. Venuti, C. D. E. Boschi, E. Ercolessi, G. Morandi, F. Ortolani, S. Pasini, and M. Roncaglia, Stable particles in anisotropic spin-1 chains, *Eur. Phys. J. B* **53**, 11 (2006).
- [20] Y.-C. Tzeng and M.-F. Yang, Scaling properties of fidelity in the spin-1 anisotropic model, *Phys. Rev. A* **77**, 012311 (2008).
- [21] Y.-C. Tzeng, H.-H. Hung, Y.-C. Chen, and M.-F. Yang, Fidelity approach to Gaussian transitions, *Phys. Rev. A* **77**, 062321 (2008).
- [22] F. Pollmann, A. M. Turner, E. Berg, and M. Oshikawa, Entanglement spectrum of a topological phase in one dimension, *Phys. Rev. B* **81**, 064439 (2010).
- [23] J. Cui, L. Amico, H. Fan, M. Gu, A. Hama, and V. Vedral, Local characterization of one-dimensional topologically ordered states, *Phys. Rev. B* **88**, 125117 (2013).
- [24] H. Bragança, E. Mascarenhas, G. I. Luiz, C. Duarte, R. G. Pereira, M. F. Santos, and M. C. O. Aguiar, Nonuniversality of entanglement convertibility, *Phys. Rev. B* **89**, 235132 (2014).
- [25] Y. Rahnavard and W. Brenig, Spin dynamics of the anisotropic spin-1 antiferromagnetic chain at finite magnetic fields, *Phys. Rev. B* **91**, 054405 (2015).
- [26] Y. Fuji, Effective field theory for one-dimensional valence-bond-solid phases and their symmetry protection, *Phys. Rev. B* **93**, 104425 (2016).
- [27] M. Kaburagi and T. Tonegawa, Effects of the single-ion-type anisotropy on the spin-1 Haldane system with a spin-1/2 impurity, *Physica B* **211**, 193 (1995).
- [28] C. Rudowicz, Effect of small in-plane anisotropy in the large- $D$  phase systems based on Ni<sup>2+</sup> ( $S = 1$ ) ions in Heisenberg antiferromagnetic chains, *Physica B* **436**, 193 (2014).
- [29] S. Chattopadhyay, D. Jain, V. Ganesan, S. Giri, and S. Majumdar, Observation of large- $D$  magnetic phase in Sr<sub>3</sub>NiPtO<sub>6</sub>, *Phys. Rev. B* **82**, 094431 (2010).
- [30] A.-M. Pradipto, R. Broer, and S. Picozzi, *Ab initio* modeling of magnetic anisotropy in Sr<sub>3</sub>NiPtO<sub>6</sub>, *Phys. Chem. Chem. Phys.* **18**, 4078 (2016).
- [31] M. Orendáč, A. Orendáčová, J. Černák, A. Feher, P. J. C. Signore, M. W. Meisel, S. Merah, and M. Verdager, Thermodynamic and magnetic properties of the  $S = 1$  Heisenberg chain Ni(C<sub>2</sub>H<sub>8</sub>N<sub>2</sub>)<sub>2</sub>Ni(CN)<sub>4</sub>: Experiments and theory, *Phys. Rev. B* **52**, 3435 (1995).
- [32] J. L. Manson, A. G. Baldwin, B. L. Scott, J. Bendix, Rico E. Del Sesto, P. A. Goddard, Y. Kohama, H. E. Tran, S. Ghannadzadeh, J. Singleton, T. Lancaster, Johannes S. Möller, S. J. Blundell, F. L. Pratt, V. S. Zapf, J. Kang, C. Lee, M.-H. Whangbo, and C. Baines, [Ni(HF<sub>2</sub>)(3-Clpy)<sub>4</sub>]BF<sub>4</sub> (py=pyridine): Evidence for spin exchange along strongly distorted FHF<sup>-</sup> bridges in a one-dimensional polymeric chain, *Inorg. Chem.* **51**, 7520 (2012).
- [33] J.-S. Xia, A. Ozarowski, P. M. Spurgeon, A. G. Baldwin, J. L. Manson, and M. W. Meisel, [arXiv:1409.5971](https://arxiv.org/abs/1409.5971).

- [34] M. Orendáč, E. Čížmár, A. Orendáčová, J. Černák, A. Feher, M. W. Meisel, K. A. Abboud, S. Zvyagin, M. Sieling, T. Rieth, and B. Lüthi, Magnetic and thermodynamic properties of  $\text{Ni}(\text{C}_{10}\text{H}_8\text{N}_2)_2\text{Ni}(\text{CN})_4 \cdot \text{H}_2\text{O}$ : A  $S = 1$  Heisenberg antiferromagnetic chain with strong in-plane anisotropy and subcritical exchange coupling, *Phys. Rev. B* **61**, 3223 (2000).
- [35] M. T. Batchelor, X.-W. Guan, and N. Oelkers, Thermal and magnetic properties of spin-1 magnetic chain compounds with large single-ion and in-plane anisotropies, *Phys. Rev. B* **70**, 184408 (2004).
- [36] M. T. Batchelor, X.-W. Guan, N. Oelkers, and A. Foerster, Thermal and magnetic properties of integrable spin-1 and spin-3/2 chains with applications to real compounds, *J. Stat. Mech.* (2004) P10017.
- [37] S. R. White, Density Matrix Formulation for Quantum Renormalization Groups, *Phys. Rev. Lett.* **69**, 2863 (1992).
- [38] See Supplemental Material at <http://link.aps.org/supplemental/10.1103/PhysRevB.96.060404> for details of numerical data and the proof of the permutation symmetry.
- [39] Y.-C. Tzeng, L. Dai, M.-C. Chung, L. Amico, and L.-C. Kwek, Entanglement convertibility by sweeping through the quantum phases of the alternating bonds XXZ chain, *Sci. Rep.* **6**, 26453 (2016).
- [40] H. Pichler, G. Zhu, A. Seif, P. Zoller, and M. Hafezi, Measurement Protocol for the Entanglement Spectrum of Cold Atoms, *Phys. Rev. X* **6**, 041033 (2016).
- [41] A. Chandran, M. Hermanns, N. Regnault, and B. A. Bernevig, Bulk-edge correspondence in entanglement spectra, *Phys. Rev. B* **84**, 205136 (2011).
- [42] X.-L. Qi, H. Katsura, and Andreas W. W. Ludwig, General Relationship Between the Entanglement Spectrum and the Edge State Spectrum of Topological Quantum States, *Phys. Rev. Lett.* **108**, 196402 (2012).
- [43] H. Li and F. D. M. Haldane, Entanglement Spectrum as a Generalization of Entanglement Entropy: Identification of Topological Order in Non-Abelian Fractional Quantum Hall Effect States, *Phys. Rev. Lett.* **101**, 010504 (2008).
- [44] S. Ejima and H. Fehske, Comparative density-matrix renormalization group study of symmetry-protected topological phases in spin-1 chain and Bose-Hubbard models, *Phys. Rev. B* **91**, 045121 (2015).
- [45] W. Li, A. Weichselbaum, and J. von Delft, Identifying symmetry-protected topological order by entanglement entropy, *Phys. Rev. B* **88**, 245121 (2013).
- [46] S. Singh, Identifying quantum phases from the injectivity of symmetric matrix product states, *Phys. Rev. B* **91**, 115145 (2015).
- [47] S. N. Saadatmand and I. P. McCulloch, Symmetry fractionalization in the topological phase of the spin- $\frac{1}{2}$   $J_1 - J_2$  triangular Heisenberg model, *Phys. Rev. B* **94**, 121111 (2016); [arXiv:1704.03418](https://arxiv.org/abs/1704.03418).
- [48] A. V. Chubukov, Chiral, nematic, and dimer states in quantum spin chains, *Phys. Rev. B* **44**, 4693(R) (1991).
- [49] T. Hikihara, L. Kecke, T. Momoi, and A. Furusaki, Vector chiral and multipolar orders in the spin-1/2 frustrated ferromagnetic chain in magnetic field, *Phys. Rev. B* **78**, 144404 (2008).
- [50] H. Onishi, Magnetic excitations of spin nematic state in frustrated ferromagnetic chain, *J. Phys. Soc. Jpn.* **84**, 083702 (2015).
- [51] H. Onishi, Effects of magnetic anisotropy on spin dynamics of ferromagnetic frustrated chain, *J. Phys.: Conf. Ser.* **592**, 012109 (2015).
- [52] T. Masuda, M. Hagihala, Y. Kondoh, K. Kaneko, and N. Metoki, Spin density wave in insulating ferromagnetic frustrated chain  $\text{LiCuVO}_4$ , *J. Phys. Soc. Jpn.* **80**, 113705 (2011).
- [53] M. Mourigal, M. Enderle, B. Fåk, R. K. Kremer, J. M. Law, A. Schneidewind, A. Hiess, and A. Prokofiev, Evidence of a Bond-Nematic Phase in  $\text{LiCuVO}_4$ , *Phys. Rev. Lett.* **109**, 027203 (2012).
- [54] L. Amico, R. Fazio, A. Osterloh, and V. Vedral, Entanglement in many-body systems, *Rev. Mod. Phys.* **80**, 517 (2008).
- [55] G. Vidal, J. I. Latorre, E. Rico, and A. Kitaev, Entanglement in Quantum Critical Phenomena, *Phys. Rev. Lett.* **90**, 227902 (2003).
- [56] V. E. Korepin, Universality of Entropy Scaling in One Dimensional Gapless Models, *Phys. Rev. Lett.* **92**, 096402 (2004).
- [57] P. Calabrese, M. Campostrini, F. Essler, and B. Nienhuis, Parity Effects in the Scaling of Block Entanglement in Gapless Spin Chains, *Phys. Rev. Lett.* **104**, 095701 (2010).
- [58] A. F. Albuquerque, C. J. Hamer, and J. Oitmaa, Quantum phase diagram and excitations for the one-dimensional  $S = 1$  Heisenberg antiferromagnet with single-ion anisotropy, *Phys. Rev. B* **79**, 054412 (2009).
- [59] S. Hu, B. Normand, X. Wang, and L. Yu, Accurate determination of the Gaussian transition in spin-1 chains with single-ion anisotropy, *Phys. Rev. B* **84**, 220402 (2011).
- [60] A. Langari, F. Pollmann, and M. Siahhatgar, Ground-state fidelity of the spin-1 Heisenberg chain with single ion anisotropy: quantum renormalization group and exact diagonalization approaches, *J. Phys.: Condens. Matter* **25**, 406002 (2013).
- [61] K. Nomura, Correlation functions of the 2D sine-Gordon model, *J. Phys. A: Math. Gen.* **28**, 5451 (1995).
- [62] A. Kitazawa, Twisted boundary conditions of quantum spin chains near the Gaussian fixed points, *Phys. A: Math. Gen.* **30**, L285 (1997).
- [63] A. Kitazawa and K. Nomura, Critical properties of  $S = 1$  bond-alternating XXZ chains and hidden  $Z_2 \times Z_2$  symmetry, *J. Phys. Soc. Jpn.* **66**, 3944 (1997).
- [64] A. Kitazawa and K. Nomura, Phase transitions of  $S = 3/2$  and  $S = 2$  XXZ spin chains with bond alternation, *J. Phys. Soc. Jpn.* **66**, 3379 (1997).
- [65] K. Nomura and A. Kitazawa,  $SU(2)/Z_2$  symmetry of the BKT transition and twisted boundary condition, *J. Phys. A: Math. Gen.* **31**, 7341 (1998).
- [66] K. Okamoto, T. Tonegawa, H. Nakano, Tôru Sakai, K. Nomura, and M. Kaburagi, How to distinguish the Haldane/Large-D state and the intermediate-D state in an  $S = 2$  quantum spin chain with the XXZ and on-site anisotropies, *J. Phys.: Conf. Ser.* **320**, 012018 (2011).
- [67] H. Suwa and S. Todo, Generalized Moment Method for Gap Estimation and Quantum Monte Carlo Level Spectroscopy, *Phys. Rev. Lett.* **115**, 080601 (2015).
- [68] P. Jacobson, T. Herden, M. Muenks, G. Laskin, O. Brovko, V. Stepanyuk, M. Ternes, and K. Kern, Quantum engineering of spin and anisotropy in magnetic molecular junctions, *Nat. Commun.* **6**, 8536 (2015).
- [69] W. Wernsdorfer, Nùria Aliaga-Alcalde, D. N. Hendrickson, and G. Christou, Exchange-biased quantum tunneling in a

- supramolecular dimer of single-molecule magnets, *Nature (London)* **416**, 406 (2002).
- [70] T. N. Nguyen, W. Wernsdorfer, M. Shiddiq, K. A. Abboud, S. Hill, and G. Christou, Supramolecular aggregates of single-molecule magnets: exchange-biased quantum tunneling of magnetization in a rectangular  $[\text{Mn}_3]_4$  tetramer, *Chem. Sci.* **7**, 1156 (2016).
- [71] A. A. Khajetoorians, M. Valentyuk, M. Steinbrecher, T. Schlenk, A. Shick, J. Kolorenc, A. I. Lichtenstein, T. O. Wehling, R. Wiesendanger, and J. Wiebe, Tuning emergent magnetism in a Hund's impurity, *Nat. Nanotechnology* **10**, 958 (2015).
- [72] L. Liu, K. Yang, Y. Jiang, B. Song, W. Xiao, L. Li, H. Zhou, Y. Wang, S. Du, M. Ouyang, W. A. Hofer, A. H. C. Neto, and H.-J. Gao, Reversible single spin control of individual magnetic molecule by hydrogen atom adsorption, *Sci. Rep.* **3**, 1210 (2013).
- [73] C. F. Hirjibehedin, C. P. Lutz, and A. J. Heinrich, Spin coupling in engineered atomic structures, *Science* **312**, 1021 (2006).
- [74] C.-Y. Lin and B. A. Jones, First-principles calculations of engineered surface spin structures, *Phys. Rev. B* **83**, 014413 (2011).
- [75] A. F. Otte, M. Ternes, S. Loth, C. P. Lutz, C. F. Hirjibehedin, and A. J. Heinrich, Spin Excitations of a Kondo-Screened Atom Coupled to a Second Magnetic Atom, *Phys. Rev. Lett.* **103**, 107203 (2009).
- [76] S. Loth, S. Baumann, C. P. Lutz, D. M. Eigler, and A. J. Heinrich, Bistability in atomic-scale antiferromagnets, *Science* **335**, 196 (2012).
- [77] A. A. Khajetoorians, M. Steinbrecher, M. Ternes, M. Bouhasoune, M. dos Santos Dias, S. Lounis, J. Wiebe, and R. Wiesendanger, Tailoring the chiral magnetic interaction between two individual atoms, *Nat. Commun.* **7**, 10620 (2016).
- [78] R. M. W. van Bijnen and T. Pohl, Quantum Magnetism and Topological Ordering via Rydberg Dressing Near Förster Resonances, *Phys. Rev. Lett.* **114**, 243002 (2015).